

# Development of a Semi-Analytical Dynamic Force Model

MARIN AKTER<sup>1,2</sup>, MOHAMMAD ABDUL ALIM<sup>1</sup>, MD. MANJURUL  
HUSSAIN<sup>3</sup>, KAZI SHAMSUNNAHAR MITA<sup>4</sup>, ANISUL HAQUE<sup>3</sup>, MD.  
MUNSUR RAHMAN<sup>3</sup>, MD. RAYHANUR RAHMAN<sup>3</sup>

<sup>1</sup>Department of Mathematics, Bangladesh University of Engineering and Technology,  
BANGLADESH

<sup>2</sup>School of Science, University of New South Wales, AUSTRALIA

<sup>3</sup> Institute of Water and Flood Management, Bangladesh University of Engineering and  
Technology, BANGLADESH

<sup>4</sup>Civil, Environmental and Ocean Engineering Department, Stevens Institute of Technology,  
Hoboken, New Jersey 07030, USA

**Abstract:** - A moving water mass generates force which is exerted on its moving path. Cyclone generated storm surge or earthquake generated tsunami are specific examples of moving water mass generated force along the coasts. In addition to human lives, these moving water masses cause severe damages to the coastal infrastructure due to tremendous force exerted on these structures. To assess the damage on these infrastructures, an essential parameter is the resultant force exerted on these structures. To evaluate the damages, there is hardly any quantitative method available to compute this force. In this paper we have developed a semi-analytical model, named as Dynamic Force Model (DFM), by using Variational Iteration Method to compute this force. We have derived the governing equation on the basis of Saint-Venant equations which are basically 1D shallow water equations derived from the Navier-Stokes equations. DFM is verified, calibrated, validated, and applied in Bangladesh coastal zone to compute dynamic thrust force due to tropical cyclone SIDR.

**Key-Words:** - Semi-analytical method, Variational Iteration Method, Moving water mass, Thrust force, Navier-Stokes equations, Saint-Venant equations.

Received: June 19, 2023. Revised: February 23, 2024. Accepted: March 21, 2024. Published: June 3, 2024.

## 1. Introduction

A moving water mass generates force due to momentum created by the water mass itself and the acceleration due to its movement. Specific examples of moving water mass are surge waves generated by cyclones and tsunami waves generated by earthquakes that strike the coast with considerable magnitude of force. Though the sources of these

moving water masses (for example storm surge and tsunami) are different, the physical characteristics of their wave propagation (in deep water), nonlinear transformation (in shallow water) and runup (land inundation) are identical [1]. Most of the damages of coastal infrastructures are due to this thrust force. To assess stability of these structures and to ensure safety of coastal populations, it is extremely important to accurately compute this thrust force.

The rapid changes in hydrodynamics near shore substantially damage infrastructures of coastal regions. So, from the major concepts of coastal engineering, storm loading [2] (wind load, waves, hydrostatic and hydrodynamic loads) and tsunami induced forces are necessary in a coastal building code. Water-related loads accompanying a coastal storm are often not adequately addressed in coastal building code, with wind generated/ induced waves producing the most critical and complex forces to which the coast and its structures are subjected [2]. Few current building codes of coastal structures such as the city and county of Honolulu Building Code (CCH); the 1997 Uniform Building Code (UBC 97); the 2000 International Building Code (IBC 2000), the SEI/ASCE 7-02 (ASCE 7), and the Federal Emergency Management Agency Coastal Construction Manual (FEMA CCM) incorporate the effects of hydrodynamic loads (surge/tsunami induced) [3]. The generalized equations of contributing force components of these codes are discussed in [1,4-5]. In these codes, computation of hydrostatic force is the multiplicative combination of gravitational acceleration and square of specific energy. Hydrodynamic force is calculated as the drag force acting on the direction of the uniform flow. But these codes have over-simplified the process of estimating the hydrodynamic loads [1]. The forces are calculated for an instantaneous velocity of moving water mass for design purposes of coastal infrastructures. But these codes neglect the non-linearity of the variation of the total force generated during a cyclone or Tsunami.

A Tsunami induced force is done by Palermo et al, 2009 [5]. In their study, they considered three parameters to define the magnitude and application of tsunami-induced forces: (i) the inundation depth; (ii) the flow velocity; and (iii) the flow direction [5]. But they did not consider the terms it may/must be nonlinear of inundation depth, flow velocity and flow direction as the parameters work together in the field.

### Research Gap

From the synthesis of the past studies related to computation of this thrust force, it is found that over simplified empirical or semi-empirical approaches

are generally adopted mainly from engineering perspectives by ignoring physics behind the generation of this force. This force should actually be calculated by solving the momentum equation by considering acceleration of moving water mass and wind stress due to cyclone effect.

*A moving water mass generates force* which is exerted on its *moving* path that obeys always a momentum equation. So, it is necessary to define the thrust force that from the beginning of a cyclone, a momentum equation should be considered. But no such studies do this way. Rather they have calculated the forces individually which are simpler. In reality, the forces are highly nonlinear and they are dependent on each other. During the derivation of thrust forces from the momentum equation, few nonlinear terms are generated which are not considered in the previous studies.

### Research Question

In this paper, it is discussed the following two points: (a) *How the thrust force generated by the moving water mass due to cyclone or tsunami can be computed by following a physics-based approach?* (b) *What type of non-linear terms at the end can be generated during the derivation of thrust force from the momentum equation by considering moving water mass and wind stress due to cyclone effect?*

In this study, a physics-based approach is applied to compute this force dynamically. Momentum equation is used as the basic governing equation which contains the force and acceleration components of moving wind and water masses. The momentum equation is based on the Saint-Venant equation which is derived from the Navier-Stokes equation. The equation is solved semi-analytically to compute the force. As mentioned before, this force, termed as dynamic thrust force, is responsible for the damages of coastal infrastructures during propagation of a cyclone and tsunami. The semi-analytical model, named as DFM, developed in this study can simulate this thrust force dynamically during propagation of a cyclone or tsunami event.

## 2. Materials and Method

### 2.1 Analytical Methods of Partial Differential Equations

A wide variety of problems in fluid mechanics are expressed by partial differential equations and they are nonlinear. Nonlinearity exists everywhere, and nature is nonlinear in general. There are many methods, such as perturbation methods, to solve nonlinear partial differential equations (PDEs). A method known as the method of separation of variables is perhaps one of the oldest systematic methods for solving partial differential equations including the wave equation. The wave equation and its methods of solution attracted the attention of many famous mathematicians including Leonhard Euler (1707–1783), James Bernoulli (1667–1748), Daniel Bernoulli (1700–1782), J.L. Lagrange (1736–1813), and Jacques Hadamard (1865–1963) (Oliviera, 2021). They discovered solutions in several different forms of partial differential equations. A well-known analytical method is the Decomposition Method which was established by Adomian. Special attention should be paid to Adomian's decomposition method [6-7] and Liao's homotopy analysis method [8]. With these methods, most PDEs can be approximately solved without linearization or weak linearization or small perturbations. However, the approximation obtained by Adomian's method could not always satisfy all its boundary conditions, leading to error near boundaries. A successful approximation of solution for partial differential equations is established with no boundary problems by Ji-Huan He [9-12] which is known as Variational Iteration Method (VIM) [13]. This method is based on analytically solving the equations that result from discretizing the spatial coordinates of a partial differential equation [14].

Governing equations formed based on Saint-Venant equations are characteristically nonlinear partial differential equations. Functional relations for some of the variables in the governing equations are not solvable analytically. Those relations are solved by the discretization method. Here, Finite difference

method is used [15]. As the equations are solved by applying coupled VIM that is analytical and discretization methods which are known as numerical. For this reason, in this study, this coupled solution method is termed as 'semi-analytical'.

### 2.2 Model Development

According to Newton's Second Law of Motion, the change of momentum per unit of time is equal to the result of all external forces applied to the moving body. In this study, we have also considered wind force exerted on the moving body. In this case, the assumptions to the development of the governing equations and its momentum equation is formed as described below.

#### 2.2.1 Assumptions to the development of Saint-Venant Equations

In Fluid Dynamics, the Saint-Venant equations [16] were formulated in the 19th century by two mathematicians, Adhémar Jean Claude Barré Saint-Venant and Bousinesque [16]. Saint-Venant equations are derived from Navier-Stokes equations [17] for shallow water conditions [18]. Navier-Stokes equations represent a general model used to model fluid flows [19-20]. On the other hand, a general flood wave for 1-D situation [19-20] can be described by the Saint-Venant equations.

During development of the Saint Venant equations, following assumptions [17] were made:

- Flow is one-dimensional.
- Flow is unsteady and non-uniform.
- Hydrostatic pressure prevails and vertical accelerations are negligible.
- Streamline curvature is small.
- Bottom slope of the channel is small.
- The fluid is incompressible.
- The gravity force is the only force which is taken into account. So, the influence of the Coriolis force is neglected.

In addition to the above assumption, following assumptions are made for this study:

- The steady uniform state of flow is expressed by Manning's equation which is used as the initial condition for solution.
- Manning's coefficient  $n$  is used to describe the resistance effects.
- Wind is considered while forming the momentum equation.

These three additional assumptions do not affect the basic governing equation.

### 2.2.2. Conservation of momentum

Inside a control volume according to the conservation of momentum, conservation of momentum can be expressed (Vreugdenhil, 1994) as:

$$\begin{aligned} & \frac{d}{dt} [\text{Momentum}] \\ & = \text{Momentum flux entering at } x \\ & - \text{Momentum flux exiting at } (x + dx) \\ & + \text{Pressure force in the rear} \\ & - \text{Pressure force ahead} \\ & + \text{Downslope gravitaional force} \\ & - \text{Frictional force along the bottom} \\ & + \text{Frictional force on water surface due to wind} \end{aligned} \quad (1)$$

Here, the computation of Momentum flux, Pressure force, Downslope gravitation force and Frictional force in the equation (1) are taken from the studies [16-17]. And the rest term, the frictional force on water surface due to wind is calculated in this study and it is described below.

If we consider  $\rho_w = \text{the water density}$   $\rho_a = \text{air density}$ , the frictional force exerted on the water surface due to cyclonic wind term is

*Frictional force on water surface*

$$\text{due to wind, } F_w = \tau_w B dx \quad (2)$$

Where, the wind shear stress,  $\tau_w = \rho_a C_w u_w^2$  i.e. wind force  $F_w = \rho_a C_w u_w^2 B dx$ ; where  $u_w$  is the wind

velocity,  $C_w$  is wind drag coefficient,  $B$  is width of channel and  $\rho_a$  is the density of air.

Hence, in differential form, the momentum equation is

$$\frac{\partial}{\partial t} (\rho_w A u) = - \frac{\partial}{\partial x} (\rho_w A u^2) - \frac{\partial F_p}{\partial x} + \rho_w g A S_0 - C_d \rho_w p u^2 + \rho_a C_w u_w^2 B \quad (3)$$

The gradient of the pressure force can be rewritten as

$$\frac{\partial F_p}{\partial x} = \frac{dF_p}{dh} \frac{\partial h}{\partial x} = \rho_w g A \frac{\partial h}{\partial x} \quad (4)$$

Again, the ratio of the cross-sectional area  $A$  over the wetted perimeter  $p$ , which has the dimension of a length, called hydraulic radius and is defined as

$$R_h = \frac{A}{p} \quad (5)$$

Here, we consider wide water body, which is much wider than the depth, the wetted perimeter is generally not much more than the width ( $p \approx B$ ), and so the hydraulic radius is approximately

$$R_h \approx \frac{A}{B} \quad (6)$$

Therefore, the equation (12) simplifies into

$$\frac{\partial u}{\partial t} + u \frac{\partial u}{\partial x} = -g \frac{\partial h}{\partial x} + g S_0 - C_d \frac{u^2}{R_h} + \frac{\rho_a}{\rho_w R_h} C_w u_w^2 \quad (7)$$

Equation (16) is called the Saint-Venant equation i.e. 1D shallow water equation.

If cyclonic wind is absent in the momentum equation, the equation (7) becomes

$$\frac{\partial u}{\partial t} + u \frac{\partial u}{\partial x} = -g \frac{\partial h}{\partial x} + g S_0 - C_d \frac{u^2}{R_h} \quad (8)$$

It also implies a 1D shallow water equation for open channel flow where cyclonic wind is absent.

In present study, all these equations are solved semi-analytically to compute spatial variation of forces exerted by the wind and water mass.

### 2.2.3. Variational Iteration Method (VIM)

In 1978, Inokuti [21] proposed a general Lagrange multiplier method to solve nonlinear problems. The main feature of the method is as follows: the solution of a mathematical problem with linearization assumption is used as initial approximation or trial-function, then a precise approximation at some special point can be obtained. Considering the following general nonlinear system,

$$Lu(t) + Nu(t) = g(t) \tag{9}$$

where  $L$  is a linear operator,  $N$  is a nonlinear operator and  $g(t)$  is a known analytical function.

Above method was modified into an iteration method [9-11, 22-23] in the following way:

$$u_{n+1} = u_n + \int_0^t \lambda \left[ Lu_n(\xi) + Nu_n(\xi) - g(\xi) \right] d\xi \tag{10}$$

where  $\lambda$  is a general Lagrange multiplier (Inokuti, 1978), which can be identified optimally via the Variational theory [12,21, 23-24], the subscript  $n$  denotes the  $n^{th}$  approximation, and  $u_n$  is considered as a restricted variation [23], i.e.  $\delta \bar{u}_n = 0$

The method is shown to solve effectively, easily, and accurately a large class of non-linear problems with approximations converging rapidly to accurate solutions.

VIM is now widely used by many researchers to solve linear and nonlinear partial differential equations. The method introduces a reliable and efficient process for a wide variety of scientific and engineering applications, linear or nonlinear, homogeneous or non-homogeneous, equations and systems of equations as well. It was shown by many authors [9-12; 25] that this method is more powerful than existing techniques such as the Adomian method

[7, 26] or perturbation method [27]. The method gives rapidly convergent successive approximations of the exact solution if such a solution exists; otherwise, a few approximations can be used for numerical purposes. The existing numerical techniques suffer from restrictive assumptions that are used to handle nonlinear terms. The VIM has no specific requirements, such as linearization, small parameters, Adomian polynomials, etc. for nonlinear operators. Another important advantage is that the VIM method is capable of greatly reducing the size of calculation while still maintaining high accuracy of the solution. Moreover, the power of the method gives it a wider applicability in handling large numbers of analytical and numerical applications.

### 2.2.4. Solution of the Governing Equation

Equations (16) and (17) which are known as Saint Venant equations can be re-written as

$$\frac{\partial u}{\partial t} + u \frac{\partial u}{\partial x} + g \frac{\partial h}{\partial x} - g s_0 + C_d \frac{u^2}{R_h} - \frac{\rho_a}{\rho_w R_h} C_w u_w^2 = 0 \tag{11}$$

$$\text{And } \frac{\partial u_n}{\partial t} + u \frac{\partial u_n}{\partial x} + g \frac{\partial \square}{\partial x} - g s_0 + C_d \frac{u_n^2}{R_\square} = 0 \tag{12}$$

Where,  $\rho_a$  is air density,  $\rho_w$  is water density,  $u_w$  is cyclonic wind speed,  $u$  is water velocity,  $C_d$  is water drag coefficient and  $C_w$  is wind drag coefficient.

We express the steady uniform state of flow by Manning's flow equation [28] as an initial condition mentioned in the assumption for the Equations (11) and (12), which means

$$u_0(x, 0) = \frac{1}{n} R_h^{2/3} S_0^{1/2} \tag{13}$$

where  $n$  is Manning's roughness coefficient and  $R_h$  is hydraulic radius of the channel.

The correction functional for Equation (11) is

$$u_{n+1} = u_n + \int_0^t \lambda(\xi) \left[ \frac{\partial u_n}{\partial \xi} + u \frac{\partial u_n}{\partial x} + g \frac{\partial h}{\partial x} - gS_0 + C_d \frac{u_n^2}{R_h} - \frac{\rho_a}{\rho_w R_h} C_w u_w^2 \right] d\xi \quad (14)$$

The stationary condition is given by

$$\lambda'(\xi) = 0$$

$$1 + \lambda'(\xi) \Big|_{\xi=t} = 0$$

(15)

Equation (15) gives  $\lambda = -1$  and substituting the value of the Lagrange multiplier into the correction functional, Equation (14) gives the iteration formula.

$$u_{n+1} = u_n - \int_0^t \left[ \frac{\partial u_n}{\partial \xi} + u \frac{\partial u_n}{\partial x} + g \frac{\partial h}{\partial x} - gS_0 + C_d \frac{u_n^2}{R_h} - \frac{\rho_a}{\rho_w R_h} C_w u_w^2 \right] d\xi \quad (16)$$

The zeroth approximations  $u_0(x, 0) = \frac{1}{n} R_h^{2/3} S_0^{1/2}$  are selected by using the given initial conditions. Following are the successive approximations,

$$u_0(x, 0) = \frac{1}{n} R_h^{2/3} S_0^{1/2} \quad (17)$$

$$u_1 = u_0 - \int_0^t \left[ \frac{\partial u_0}{\partial \xi} + u_0 \frac{\partial u_0}{\partial x} + g \frac{\partial h}{\partial x} - gS_0 + C_d \frac{u_0^2}{R_h} - \frac{\rho_a}{\rho_w R_h} C_w u_w^2 \right] d\xi \quad (18)$$

$$u_1 = \frac{1}{n} R_h^{2/3} S_0^{1/2} - \int_0^t \left[ \frac{\partial}{\partial \xi} \left( \frac{1}{n} R_h^{2/3} S_0^{1/2} \right) + \frac{1}{n} R_h^{2/3} S_0^{1/2} * \frac{\partial}{\partial x} \left( \frac{1}{n} R_h^{2/3} S_0^{1/2} \right) + g \frac{\partial h}{\partial x} - gS_0 + C_d \frac{1}{R_h} \left( \frac{1}{n} R_h^{2/3} S_0^{1/2} \right)^2 - \frac{\rho_a}{\rho_w R_h} C_w u_w^2 \right] d\xi \quad (19)$$

$$u_1 = \frac{1}{n} R_h^{2/3} S_0^{1/2} - \int \left[ g \frac{\partial \square}{\partial x} - gS_0 + C_d \frac{1}{R_h} \left( \frac{1}{n} R_h^{2/3} S_0^{1/2} \right)^2 - \frac{\rho_a}{\rho_w R_h} C_w u_w^2 \right] d\xi$$

(20)

$$\text{as } \frac{\partial}{\partial x} \left( \frac{1}{n} R_h^{2/3} S_0^{1/2} \right) = \frac{\partial}{\partial \xi} \left( \frac{1}{n} R_h^{2/3} S_0^{1/2} \right) = 0$$

is the steady and uniform condition.

$$u_2 = u_1 - \int_0^t \left[ \frac{\partial u_1}{\partial \xi} + u_1 \frac{\partial u_1}{\partial x} + g \frac{\partial \square}{\partial x} - gS_1 + C_d \frac{u_1^2}{R_h} - \frac{\rho_a}{\rho_w R_h} C_w u_w^2 \right] d\xi \quad (21)$$

Using Equation (20), we get the 2<sup>nd</sup> iterated formula as

$$u_2 \approx \frac{1}{n} R_h^{2/3} S_0^{1/2} - \frac{1}{n} R_h^{2/3} S_0^{1/2} \left( \sum_{\xi=0}^t g \frac{\partial^2 \square}{\partial x^2} \Delta \xi^2 - \frac{2\rho_a C_w}{\rho_w R_h} \sum_{\xi=0}^t u_w \frac{\partial u_w}{\partial x} \Delta \xi^2 \right) + \left( \sum_{\xi=0}^t g \frac{\partial \square}{\partial x} \Delta \xi^2 - gS_0 t^2 + \frac{C_d}{n^2} R_h^{1/3} S_0 t^2 - \frac{\rho_a C_w}{\rho_w R_h} \sum_{\xi=0}^t u_w^2 \Delta \xi^2 \right) \left( \sum_{\xi=0}^t g \frac{\partial^2 \square}{\partial x^2} \Delta \xi - \frac{2\rho_a C_w}{\rho_w R_h} \sum_{\xi=0}^t u_w \frac{\partial u_w}{\partial x} \Delta \xi \right) - \left( \sum_{\xi=0}^t g \frac{\partial \square}{\partial x} \Delta \xi - gS_0 t + \frac{C_d}{n^2} R_h^{1/3} S_0 t - \frac{\rho_a C_w}{\rho_w R_h} \sum_{\xi=0}^t u_w^2 \Delta \xi \right)$$

$$\begin{aligned}
 & + \frac{2C_d}{n} R_{\square}^{-1/3} S_0^{1/2} \left( \sum_{\xi=0}^t g \frac{\partial \square}{\partial x} \Delta \xi^2 - g S_0 t^2 \right. \\
 & \quad \left. + \frac{C_d}{n^2} R_{\square}^{1/3} S_0 t^2 \right. \\
 & \quad \left. - \frac{\rho_a C_w}{\rho_w R_{\square}} \sum_{\xi=0}^t u_w^2 \Delta \xi^2 \right) - \\
 & \frac{2C_d}{R_{\square}} \left( \sum_{\xi=0}^t g \frac{\partial \square}{\partial x} \Delta \xi - g S_0 t + \frac{C_d}{n^2} R_{\square}^{1/3} S_0 t \right. \\
 & \quad \left. - \frac{\rho_a C_w}{\rho_w R_{\square}} \sum_{\xi=0}^t u_w^2 \Delta \xi \right)^2 \Delta \xi \\
 & \quad + \frac{\rho_a C_w}{\rho_w R_{\square}} \sum_{\xi=0}^t u_w^2 \Delta \xi
 \end{aligned} \tag{22}$$

**Definite integral**

If a function  $f(x)$  is continuous on the interval  $[a, b]$  which is divided into  $n$  subintervals of equal width  $\Delta x$ , the definite integral of  $f(x)$  from  $a$  to  $b$  is

$$\int_a^b f(x) dx \approx \lim_{n \rightarrow \infty} \sum_{i=1}^n f(x_i) \Delta x \tag{23}$$

Using definite integral, we have

$$\int_0^t g \frac{\partial h}{\partial x} d\xi \approx \sum_{\xi=0}^t g \frac{\partial h}{\partial x} \Delta \xi \text{ and } \int_0^t u_w d\xi \approx \sum_{\xi=0}^t u_w \Delta \xi \tag{24}$$

Equation (22) is simplified into

$$\begin{aligned}
 u_2 \approx & \frac{1}{n} R_{\square}^{2/3} S_0^{1/2} \\
 & - \frac{1}{n} R_{\square}^{2/3} S_0^{1/2} \left( \sum_{\xi=0}^t g \frac{\partial^2 \square}{\partial x^2} \Delta \xi^2 \right. \\
 & \left. - \frac{2\rho_a C_w}{\rho_w R_{\square}} \sum_{\xi=0}^t u_w \frac{\partial u_w}{\partial x} \Delta \xi^2 \right) +
 \end{aligned}$$

$$\begin{aligned}
 & \left( \sum_{\xi=0}^t g \frac{\partial \square}{\partial x} \Delta \xi^2 - g S_0 t^2 + \frac{C_d}{n^2} R_{\square}^{1/3} S_0 t^2 \right. \\
 & \quad \left. - \frac{\rho_a C_w}{\rho_w R_{\square}} \sum_{\xi=0}^t u_w^2 \Delta \xi^2 \right) \\
 & \left( \sum_{\xi=0}^t g \frac{\partial^2 \square}{\partial x^2} \Delta \xi - \frac{2\rho_a C_w}{\rho_w R_{\square}} \sum_{\xi=0}^t u_w \frac{\partial u_w}{\partial x} \Delta \xi \right) \\
 & - \left( \sum_{\xi=0}^t g \frac{\partial \square}{\partial x} \Delta \xi - g S_0 t + \frac{C_d}{n^2} R_{\square}^{1/3} S_0 t \right. \\
 & \quad \left. - \frac{\rho_a C_w}{\rho_w R_{\square}} \sum_{\xi=0}^t u_w^2 \Delta \xi \right) \\
 & + \frac{2C_d}{n} R_{\square}^{-1/3} S_0^{1/2} \left( \sum_{\xi=0}^t g \frac{\partial \square}{\partial x} \Delta \xi^2 - g S_0 t^2 \right. \\
 & \quad \left. + \frac{C_d}{n^2} R_{\square}^{1/3} S_0 t^2 \right. \\
 & \quad \left. - \frac{\rho_a C_w}{\rho_w R_{\square}} \sum_{\xi=0}^t u_w^2 \Delta \xi^2 \right) - \\
 & \frac{2C_d}{R_{\square}} \left( \sum_{\xi=0}^t g \frac{\partial \square}{\partial x} \Delta \xi - g S_0 t + \frac{C_d}{n^2} R_{\square}^{1/3} S_0 t - \right. \\
 & \quad \left. \frac{\rho_a C_w}{\rho_w R_{\square}} \sum_{\xi=0}^t u_w^2 \Delta \xi \right)^2 \Delta \xi + \frac{\rho_a C_w}{\rho_w R_{\square}} \sum_{\xi=0}^t u_w^2 \Delta \xi
 \end{aligned} \tag{25}$$

Equation (25) is the approximate solution of Saint-Venant equation (Equation (11)) to compute velocity  $u$  (including water depth and wind speed), i.e.  $u \approx u_2$

Therefore,

$$\begin{aligned}
 u \approx & \frac{1}{n} R_{\square}^{2/3} S_0^{1/2} \\
 & - \frac{1}{n} R_{\square}^{2/3} S_0^{1/2} \left( \sum_{\xi=0}^t g \frac{\partial^2 \square}{\partial x^2} \Delta \xi^2 \right. \\
 & \left. - \frac{2\rho_a C_w}{\rho_w R_{\square}} \sum_{\xi=0}^t u_w \frac{\partial u_w}{\partial x} \Delta \xi^2 \right) +
 \end{aligned}$$

$$\begin{aligned}
 & \left( \sum_{\xi=0}^t g \frac{\partial \square}{\partial x} \Delta \xi^2 - g S_0 t^2 + \frac{C_d}{n^2} R_{\square}^{1/3} S_0 t^2 \right. \\
 & \quad \left. - \frac{\rho_a C_w}{\rho_w R_{\square}} \sum_{\xi=0}^t u_w^2 \Delta \xi^2 \right) \\
 & \left( \sum_{\xi=0}^t g \frac{\partial^2 \square}{\partial x^2} \Delta \xi - \frac{2\rho_a C_w}{\rho_w R_{\square}} \sum_{\xi=0}^t u_w \frac{\partial u_w}{\partial x} \Delta \xi \right) \\
 & - \left( \sum_{\xi=0}^t g \frac{\partial \square}{\partial x} \Delta \xi - g S_0 t + \frac{C_d}{n^2} R_{\square}^{1/3} S_0 t \right. \\
 & \quad \left. - \frac{\rho_a C_w}{\rho_w R_{\square}} \sum_{\xi=0}^t u_w^2 \Delta \xi \right) \\
 & + \frac{2C_d}{n} R_{\square}^{-1/3} S_0^{1/2} \left( \sum_{\xi=0}^t g \frac{\partial \square}{\partial x} \Delta \xi^2 - g S_0 t^2 \right. \\
 & \quad \left. + \frac{C_d}{n^2} R_{\square}^{1/3} S_0 t^2 \right. \\
 & \quad \left. - \frac{\rho_a C_w}{\rho_w R_{\square}} \sum_{\xi=0}^t u_w^2 \Delta \xi^2 \right) - \\
 & \frac{2C_d}{R_{\square}} \left( \sum_{\xi=0}^t g \frac{\partial \square}{\partial x} \Delta \xi - g S_0 t + \frac{C_d}{n^2} R_{\square}^{1/3} S_0 t \right. \\
 & \quad \left. - \frac{\rho_a C_w}{\rho_w R_{\square}} \sum_{\xi=0}^t u_w^2 \Delta \xi \right)^2 \Delta \xi \\
 & + \frac{\rho_a C_w}{\rho_w R_{\square}} \sum_{\xi=0}^t u_w^2 \Delta \xi
 \end{aligned} \tag{26}$$

If we do not consider any wind term in the momentum equation, the solution becomes

$$u \approx \frac{1}{n} R_{\square}^{2/3} S_0^{1/2} - \frac{1}{n} R_{\square}^{2/3} S_0^{1/2} \left( \sum_{\xi=0}^t g \frac{\partial^2 \square}{\partial x^2} \Delta \xi \right) +$$

$$\begin{aligned}
 & \left( \sum_{\xi=0}^t g \frac{\partial \square}{\partial x} \Delta \xi^2 - g S_0 t^2 \right. \\
 & \quad \left. + \frac{C_d}{n^2} R_{\square}^{1/3} S_0 t^2 \right) \left( \sum_{\xi=0}^t g \frac{\partial^2 \square}{\partial x^2} \Delta \xi \right) \\
 & - \\
 & \left( \sum_{\xi=0}^t g \frac{\partial \square}{\partial x} \Delta \xi - g S_0 t + \frac{C_d}{n^2} R_{\square}^{1/3} S_0 t \right) \\
 & + \frac{2C_d}{n} R_{\square}^{-1/3} S_0^{1/2} \left( \sum_{\xi=0}^t g \frac{\partial \square}{\partial x} \Delta \xi^2 \right. \\
 & \quad \left. - g S_0 t^2 + \frac{C_d}{n^2} R_{\square}^{1/3} S_0 t^2 \right) \\
 & - \frac{2C_d}{R_{\square}} \left( \sum_{\xi=0}^t g \frac{\partial \square}{\partial x} \Delta \xi - g S_0 t + \frac{C_d}{n^2} R_{\square}^{1/3} S_0 t \right)^2 \Delta \xi
 \end{aligned} \tag{27}$$

Equation (27) is the approximate solution of Saint-Venant equation (when wind speed is absent) given by Equation (12).

### 2.3 Computation of Dynamic Thrust Force

Let  $u(x, t)$  denotes the water velocity (computed by using water depth and wind speed as input) at spatial location  $x$  and temporal state  $t$ .

If a water particle travels along the curve through the water body, the rate of change of velocity creates two kinds of accelerations: (a) Local acceleration and (b) Convective acceleration. It is worth mentioning that a force produced from the moving body affected by both wind and water mass is called thrust force in this study.

The acceleration for water particle can be calculated by using

$$a = \frac{\partial u}{\partial t} + u \frac{\partial u}{\partial x} \tag{28}$$

where,  $\frac{\partial u}{\partial t}$  is called local acceleration i.e temporal variation and  $u \frac{\partial u}{\partial x}$  is called convective acceleration when the particles move through regions with spatially varying velocity.

Since the water under consideration is moving, it is acted upon by external forces which will follow Newton's second law. i.e.  $F = ma$

Therefore, the force for moving fluid (Yazar, et.al., 2024) can be calculated as

$$F = \rho A \left( \frac{\partial u}{\partial t} + u \frac{\partial u}{\partial x} \right) \tag{29}$$

which is considered as the dynamic thrust force due to cyclone generated surge wave.

Using Equation (26), we can compute the local acceleration as

$$\begin{aligned} \frac{\partial u}{\partial t} \approx & -\frac{1}{n} R_{\square}^{2/3} S_0^{1/2} \left( \sum_{\xi=0}^t g \frac{\partial^2 \square}{\partial x^2} \Delta \xi \right. \\ & \left. - \frac{2\rho_a C_w}{\rho_w R_{\square}} \sum_{\xi=0}^t u_w \frac{\partial u_w}{\partial x} \Delta \xi \right) + \\ & \left( \sum_{\xi=0}^t g \frac{\partial \square}{\partial x} \Delta \xi^2 - g S_0 t^2 + \frac{C_d}{n^2} R_{\square}^{1/3} S_0 t^2 \right. \\ & \left. - \frac{C_w \rho_a}{\rho_w R_{\square}} \sum_{\xi=0}^t u_w^2 \Delta \xi^2 \right) \\ & \left( \sum_{\xi=0}^t g \frac{\partial^2 \square}{\partial x^2} \Delta \xi - \frac{2\rho_a C_w}{\rho_w R_{\square}} \sum_{\xi=0}^t u_w \frac{\partial u_w}{\partial x} \Delta \xi \right) \\ & - \left( g \frac{\partial \square}{\partial x} - g S_0 + \frac{C_d}{n^2} R_{\square}^{1/3} S_0 \right. \\ & \left. - \frac{C_w \rho_a}{\rho_w R_{\square}} u_w^2 \right) + \end{aligned}$$

$$\begin{aligned} & \frac{2C_d}{n} R_{\square}^{-1/3} S_0^{1/2} \left( \sum_{\xi=0}^t g \frac{\partial \square}{\partial x} \Delta \xi^2 - g S_0 t^2 \right. \\ & \left. + \frac{C_d}{n^2} R_{\square}^{1/3} S_0 t^2 \right. \\ & \left. - \frac{C_w \rho_a}{\rho_w R_{\square}} \sum_{\xi=0}^t u_w^2 \Delta \xi^2 \right) - \\ & \frac{C_d}{R_{\square}} \left( \sum_{\xi=0}^t g \frac{\partial \square}{\partial x} \Delta \xi^2 - g S_0 t^2 + \frac{C_d}{n^2} R_{\square}^{1/3} S_0 t^2 - \right. \\ & \left. \frac{C_w \rho_a}{\rho_w R_{\square}} \sum_{\xi=0}^t u_w^2 \Delta \xi^2 \right)^2 \end{aligned} \tag{30}$$

Again, using Equation (26), we can compute the convective acceleration as

$$\begin{aligned} \frac{\partial u}{\partial x} \approx & -\frac{1}{n} R_{\square}^{2/3} S_0^{1/2} \left( \sum_{\xi=0}^t g \frac{\partial^3 \square}{\partial x^3} \Delta \xi^3 \right. \\ & \left. - \frac{2\rho_a C_w}{\rho_w R_{\square}} \sum_{\xi=0}^t u_w \frac{\partial^2 u_w}{\partial x^2} \Delta \xi^2 \right. \\ & \left. - \frac{2\rho_a C_w}{\rho_w R_{\square}} \sum_{\xi=0}^t u_w \left( \frac{\partial u_w}{\partial x} \right)^2 \Delta \xi^2 \right) + \\ & \left( \sum_{\xi=0}^t g \frac{\partial^2 \square}{\partial x^2} \Delta \xi \right. \\ & \left. - \frac{2\rho_a C_w}{\rho_w R_{\square}} \sum_{\xi=0}^t u_w \frac{\partial u_w}{\partial x} \Delta \xi \right) \left( \sum_{\xi=0}^t g \frac{\partial^2 \square}{\partial x^2} \Delta \xi^2 \right. \\ & \left. - \frac{2\rho_a C_w}{\rho_w R_{\square}} \sum_{\xi=0}^t u_w \frac{\partial u_w}{\partial x} \Delta \xi^2 \right) \\ & \left( \sum_{\xi=0}^t g \frac{\partial^3 \square}{\partial x^3} \Delta \xi^3 - \frac{2\rho_a C_w}{\rho_w R_{\square}} \sum_{\xi=0}^t u_w \frac{\partial^2 u_w}{\partial x^2} \Delta \xi^2 \right. \\ & \left. - \frac{2\rho_a C_w}{\rho_w R_{\square}} \sum_{\xi=0}^t u_w \left( \frac{\partial u_w}{\partial x} \right)^2 \Delta \xi^2 \right) \\ & \left( \sum_{\xi=0}^t g \frac{\partial \square}{\partial x} \Delta \xi - \sum_{\xi=0}^t g \frac{\partial z}{\partial x} \Delta \xi + \frac{C_d}{n^2} R_{\square}^{1/3} S_0 \right. \\ & \left. - \frac{\rho_a C_w}{\rho_w R_{\square}} \sum_{\xi=0}^t u_w^2 \Delta \xi \right) \end{aligned}$$

$$\begin{aligned}
 & - \left( \sum_{\xi=0}^t g \frac{\partial^2 \square}{\partial x^2} \Delta \xi - \frac{2\rho_a C_w}{\rho_w R_{\square}} \sum_{\xi=0}^t u_w \frac{\partial u_w}{\partial x} \Delta \xi \right) \\
 & \quad + \frac{2C_d}{n} R_{\square}^{-1/3} S_0^{1/2} \\
 & \left( \sum_{\xi=0}^t g \frac{\partial^2 \square}{\partial x^2} \Delta \xi^2 - \frac{2\rho_a C_w}{\rho_w R_{\square}} \sum_{\xi=0}^t u_w \frac{\partial u_w}{\partial x} \Delta \xi^2 \right) - \\
 & \frac{2C_d}{R_{\square}} \left( \sum_{\xi=0}^t g \frac{\partial \square}{\partial x} \Delta \xi \right. \\
 & \quad - \sum_{\xi=0}^t g \frac{\partial z}{\partial x} \Delta \xi + \frac{C_d}{n^2} R_{\square}^{1/3} S_0 \\
 & \quad \left. - \frac{\rho_a C_w}{\rho_w R_{\square}} \sum_{\xi=0}^t u_w^2 \Delta \xi \right) \\
 & \left( \sum_{\xi=0}^t g \frac{\partial^2 \square}{\partial x^2} \Delta \xi^2 - \frac{2\rho_a C_w}{\rho_w R_{\square}} \sum_{\xi=0}^t u_w \frac{\partial u_w}{\partial x} \Delta \xi^2 \right)
 \end{aligned} \tag{31}$$

Now we can write the Equation (29) as

$$\begin{aligned}
 F = \rho A \left[ \left\{ -\frac{1}{n} R_{\square}^{2/3} S_0^{1/2} \left( \sum_{\xi=0}^t g \frac{\partial^2 \square}{\partial x^2} \Delta \xi \right. \right. \right. \\
 \left. \left. - \frac{2\rho_a C_w}{\rho_w R_{\square}} \sum_{\xi=0}^t u_w \frac{\partial u_w}{\partial x} \Delta \xi \right) \right\} + \\
 \left( \sum_{\xi=0}^t g \frac{\partial \square}{\partial x} \Delta \xi^2 - g S_0 t^2 + \frac{C_d}{n^2} R_{\square}^{1/3} S_0 t^2 \right. \\
 \left. - \frac{C_w \rho_a}{\rho_w R_{\square}} \sum_{\xi=0}^t u_w^2 \Delta \xi^2 \right) \left( \sum_{\xi=0}^t g \frac{\partial^2 \square}{\partial x^2} \Delta \xi - \right. \\
 \left. \frac{2\rho_a C_w}{\rho_w R_{\square}} \sum_{\xi=0}^t u_w \frac{\partial u_w}{\partial x} \Delta \xi \right) - \\
 \left( g \frac{\partial \square}{\partial x} - g S_0 + \frac{C_d}{n^2} R_{\square}^{1/3} S_0 - \frac{C_w \rho_a}{\rho_w R_{\square}} u_w^2 \right) \\
 \left. + \frac{2C_d}{n} R_{\square}^{-1/3} S_0^{1/2} \right)
 \end{aligned}$$

$$\begin{aligned}
 & \left( \sum_{\xi=0}^t g \frac{\partial \square}{\partial x} \Delta \xi^2 - g S_0 t^2 + \frac{C_d}{n^2} R_{\square}^{1/3} S_0 t^2 \right. \\
 & \quad \left. - \frac{C_w \rho_a}{\rho_w R_{\square}} \sum_{\xi=0}^t u_w^2 \Delta \xi^2 \right) - \\
 & \frac{C_d}{R_{\square}} \left( \sum_{\xi=0}^t g \frac{\partial \square}{\partial x} \Delta \xi - g S_0 t + \frac{C_d}{n^2} R_{\square}^{1/3} S_0 t \right. \\
 & \quad \left. - \frac{C_w \rho_a}{\rho_w R_{\square}} \sum_{\xi=0}^t u_w^2 \Delta \xi \right)^2 \\
 & \quad + u \left\{ -\frac{1}{n} R_{\square}^{2/3} S_0^{1/2} \right. \\
 & \left. \left( \sum_{\xi=0}^t g \frac{\partial^3 \square}{\partial x^3} \Delta \xi - \frac{2\rho_a C_w}{\rho_w R_{\square}} \sum_{\xi=0}^t u_w \frac{\partial^2 u_w}{\partial x^2} \Delta \xi^2 \right. \right. \\
 & \quad \left. \left. - \frac{2C_w \rho_a}{\rho_w R_{\square}} \sum_{\xi=0}^t u_w \left( \frac{\partial u_w}{\partial x} \right)^2 \Delta \xi^2 \right) \right\} + \\
 & \left( \sum_{\xi=0}^t g \frac{\partial^2 \square}{\partial x^2} \Delta \xi \right. \\
 & \quad \left. - \frac{2\rho_a C_w}{\rho_w R_{\square}} \sum_{\xi=0}^t u_w \frac{\partial u_w}{\partial x} \Delta \xi \right) \left( \sum_{\xi=0}^t g \frac{\partial^2 \square}{\partial x^2} \Delta \xi^2 \right. \\
 & \quad \left. - \frac{2\rho_a C_w}{\rho_w R_{\square}} \sum_{\xi=0}^t u_w \frac{\partial u_w}{\partial x} \Delta \xi^2 \right) + \\
 & \left( \sum_{\xi=0}^t g \frac{\partial^3 \square}{\partial x^3} \Delta \xi - \frac{2\rho_a C_w}{\rho_w R_{\square}} \sum_{\xi=0}^t u_w \frac{\partial^2 u_w}{\partial x^2} \Delta \xi^2 \right. \\
 & \quad \left. - \frac{2C_w \rho_a}{\rho_w R_{\square}} \sum_{\xi=0}^t u_w \left( \frac{\partial u_w}{\partial x} \right)^2 \Delta \xi^2 \right) \\
 & \left( \sum_{\xi=0}^t g \frac{\partial \square}{\partial x} \Delta \xi + \frac{C_d}{n^2} R_{\square}^{1/3} S_0 - \frac{C_w \rho_a}{\rho_w R_{\square}} \sum_{\xi=0}^t u_w^2 \Delta \xi \right) \\
 & \quad - \left( \sum_{\xi=0}^t g \frac{\partial^2 \square}{\partial x^2} \Delta \xi \right. \\
 & \quad \left. - \frac{2\rho_a C_w}{\rho_w R_{\square}} \sum_{\xi=0}^t u_w \frac{\partial u_w}{\partial x} \Delta \xi \right) +
 \end{aligned}$$

$$\begin{aligned} & \frac{2C_d}{n} R_{\square}^{-1/3} S_0^{1/2} \left( \sum_{\xi=0}^t g \frac{\partial^2 \square}{\partial x^2} \Delta \xi^2 \right. \\ & \quad \left. - \frac{2\rho_a C_w}{\rho_w R_{\square}} \sum_{\xi=0}^t u_w \frac{\partial u_w}{\partial x} \Delta \xi^2 \right) - \frac{2C_d}{R_{\square}} \\ & \left( \sum_{\xi=0}^t g \frac{\partial \square}{\partial x} \Delta \xi + \frac{C_d}{n^2} R_{\square}^{1/3} S_0 t \right. \\ & \quad \left. - \frac{C_w \rho_a}{\rho_w R_{\square}} \sum_{\xi=0}^t u_w^2 \Delta \xi \right) \left( \sum_{\xi=0}^t g \frac{\partial^2 \square}{\partial x^2} \Delta \xi^2 \right. \\ & \quad \left. - \frac{2\rho_a C_w}{\rho_w R_{\square}} \sum_{\xi=0}^t u_w \frac{\partial u_w}{\partial x} \Delta \xi^2 \right) \Bigg] \end{aligned} \tag{32}$$

Where,

$$\begin{aligned} u & \approx \frac{1}{n} R_{\square}^{2/3} S_0^{1/2} \\ & - \frac{1}{n} R_{\square}^{2/3} S_0^{1/2} \left( \sum_{\xi=0}^t g \frac{\partial^2 \square}{\partial x^2} \Delta \xi^2 \right. \\ & \quad \left. - \frac{2\rho_a C_w}{\rho_w R_{\square}} \sum_{\xi=0}^t u_w \frac{\partial u_w}{\partial x} \Delta \xi^2 \right) + \\ & \left( \sum_{\xi=0}^t g \frac{\partial \square}{\partial x} \Delta \xi^2 - g S_0 t^2 + \frac{C_d}{n^2} R_{\square}^{1/3} S_0 t^2 \right. \\ & \quad \left. - \frac{\rho_a C_w}{\rho_w R_{\square}} \sum_{\xi=0}^t u_w^2 \Delta \xi^2 \right) \\ & \left( \sum_{\xi=0}^t g \frac{\partial^2 \square}{\partial x^2} \Delta \xi - \frac{2\rho_a C_w}{\rho_w R_{\square}} \sum_{\xi=0}^t u_w \frac{\partial u_w}{\partial x} \Delta \xi \right) \\ & - \left( \sum_{\xi=0}^t g \frac{\partial \square}{\partial x} \Delta \xi - g S_0 t + \frac{C_d}{n^2} R_{\square}^{1/3} S_0 t \right. \\ & \quad \left. - \frac{\rho_a C_w}{\rho_w R_{\square}} \sum_{\xi=0}^t u_w^2 \Delta \xi \right) \end{aligned}$$

$$\begin{aligned} & + \frac{2C_d}{n} R_{\square}^{-1/3} S_0^{1/2} \left( \sum_{\xi=0}^t g \frac{\partial \square}{\partial x} \Delta \xi^2 - g S_0 t^2 \right. \\ & \quad \left. + \frac{C_d}{n^2} R_{\square}^{1/3} S_0 t^2 \right. \\ & \quad \left. - \frac{\rho_a C_w}{\rho_w R_{\square}} \sum_{\xi=0}^t u_w^2 \Delta \xi^2 \right) - \\ & \frac{2C_d}{R_{\square}} \left( \sum_{\xi=0}^t g \frac{\partial \square}{\partial x} \Delta \xi - g S_0 t + \frac{C_d}{n^2} R_{\square}^{1/3} S_0 t - \right. \\ & \quad \left. \frac{\rho_a C_w}{\rho_w R_{\square}} \sum_{\xi=0}^t u_w^2 \Delta \xi \right)^2 \Delta \xi + \frac{\rho_a C_w}{\rho_w R_{\square}} \sum_{\xi=0}^t u_w^2 \Delta \xi \end{aligned} \tag{33}$$

Equation (32) is the required equation to calculate the dynamic thrust force due to momentum created by the wind and water mass. In present study, these are used to compute the dynamic thrust force exerted by the cyclone generated storm surge. The model represented by Equations (32) and (33) is named as Dynamic Force Model (DFM).

Equations (32) and (33) contain the derivatives  $\frac{\partial h}{\partial x}$ ,  $\frac{\partial u_w}{\partial x}$ ,  $\frac{\partial^2 h}{\partial x^2}$  and  $\frac{\partial^2 u_w}{\partial x^2}$  that are solved numerically using finite difference method [15] and their discretized forms are written as:

$$\frac{\partial \square}{\partial x} = \frac{\square_i - \square_{i-1}}{\Delta x} \tag{34}$$

$$\frac{\partial u_w}{\partial x} = \frac{u_{wi} - u_{wi-1}}{\Delta x} \tag{35}$$

$$\frac{\partial^2 \square}{\partial x^2} = \frac{\square_i - 2\square_{i-1} + \square_{i+1}}{2\Delta x} \tag{36}$$

$$\frac{\partial^2 u_w}{\partial x^2} = \frac{u_{wi} - 2u_{wi-1} + u_{wi+1}}{2\Delta x} \tag{37}$$

Here  $i = 1, 2, 3, \dots$ . Though the governing equation of the DFM model is solved analytically (Variational Iteration Method), some forms are computed numerically (Finite Difference Method). For this reason, it is termed as semi-analytical model.

To make the DFM directly coupled with Delft 3D [29], water depth  $h$ , wind velocity  $u_w$  and discretization interval  $\Delta x$  computed from Delft 3D are directly inserted in Equations (32) and (33) it is to be noted here that any numerical model in lieu of Delft 3D can be coupled with DFM.

### 3. Model Verification

Model verification essentially means “model algorithm and code are correctly implemented” [30]. In this study, the solution algorithm and model code are verified by comparing the semi-analytical model results with the numerical solution. We use the Variational Iteration Method as an analytical method. To verify this semi-analytical solution, the numerical method selected is the Finite Difference Method [15]. The reflexive condition is used as boundary conditions during the numerical solution. Using MATLAB, we have prepared two scripts for the semi-analytical solution and the numerical solution separately. During comparison, only the velocity computed from the DFM is compared with the numerical solution of the governing equation from which the velocity field is also calculated. This essentially serves the purpose of model verification.

#### 3.1 Numerical solution using finite difference method

Finite difference method [31] is considered as a numerical method for the solutions of the governing equation (11).

To verify the DFM algorithm and code, the velocity field computed by the Equation (26) is compared with the velocity field computed from numerical solution of the governing equation (11) in a hypothetical channel where water is flowing from upstream to downstream.

##### 3.1.1 Hypothetical channel description

A hypothetical channel of 5.1km long, 100m width and 5m deep is considered for verification of the model (Fig. 1). Winds with variable speeds are assumed to blow over the channel. Steady and uniform state of flow represented by Manning’s equation i.e.  $u_0 = \frac{1}{n} R_h^{2/3} S_0^{1/2}$  is used as initial

condition, where  $R_h$  is the hydraulic radius and  $S_0$  is the bed slope of the channel.

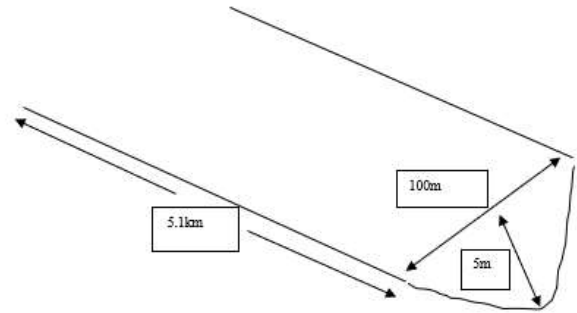


Fig. 1: Hypothetical channel

3 different cases (Case-1, Case-2 and Case-3) are constructed to compare the velocities computed by DFM with the numerical solution. In Case-1, water depth and water surface slope are kept constant (Fig. 2) with no wind blowing over the channel. This results in almost constant water velocity along the channel. Computed water velocities from the DFM and the numerical solution are shown in Fig. 3. The result shows a near perfect agreement between the DFM and the numerical solution with  $R^2=0.96$ .

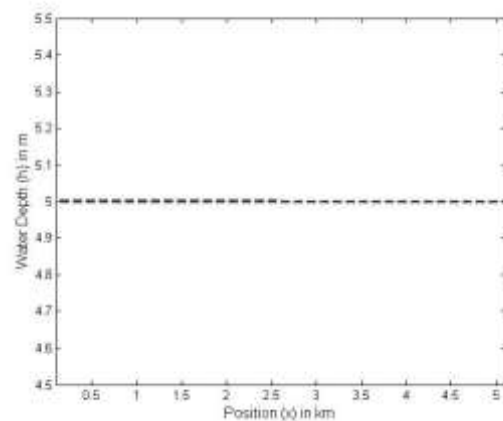


Fig. 2: Water depths  $h$ (m) in different positions  $x$ (km) along the horizontal for Case-1.

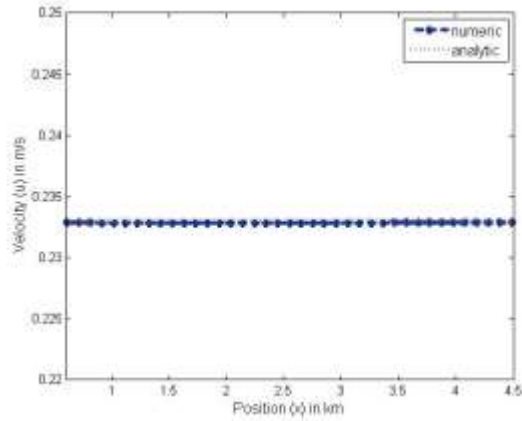


Fig. 3: Comparison of longitudinal velocity profile  $u$ (m/s) between the DFM and the numerical solution for Case-1.

In Case-2, water depth is varying along the channel, but no wind is blowing (Fig. 4). This results in variable water surface gradients along the channel. Comparison of computed water velocity between the DFM and the numerical solution is shown in Fig. 5. The result shows a slight decrease of agreement between the DFM and the numerical solution compared to Case-1 ( $R^2$  decreases from 0.96 to 0.91).

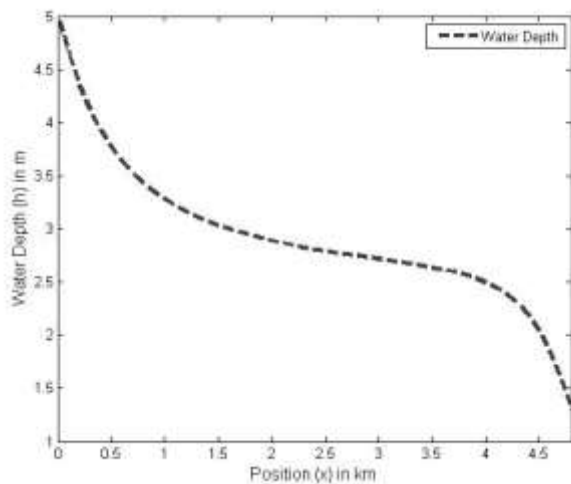


Fig. 4: Water depths  $h$ (m) in different positions  $x$ (km) along the horizontal for Case-2.

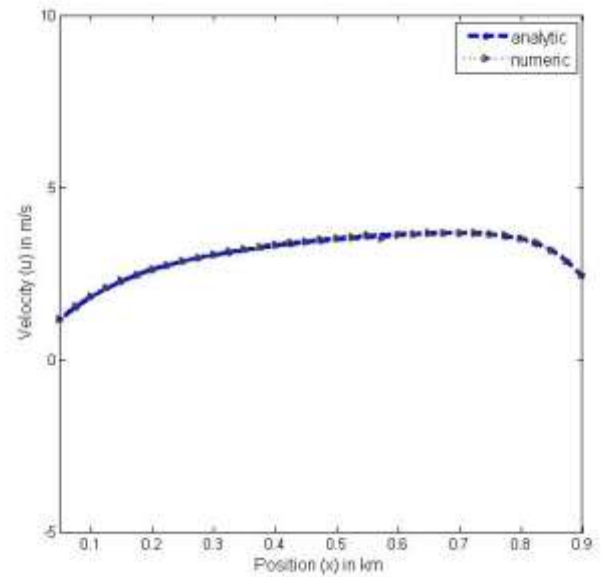


Fig. 5: Comparison of longitudinal velocity profile  $u$ (m/s) between the DFM and the numerical solution for Case-2.

In Case-3, wind with variable speed is assumed to blow over the channel where water depth was initially constant (Fig. 6). Variable wind speed results change in water surface gradient along the channel. Comparison of water velocity between the DFM and the numerical solution for Case-3 is shown in Fig. 7. The result shows further decrease of agreement between the DFM and the numerical solution compared to Case-1 and Case-2 ( $R^2=0.82$  in Case-3 compared to 0.96 in Case-1 and 0.91 in Case-2).

The verification results show systematic deviation of numerical solution from the analytical solution with the increase of non-linearity in the system, which is an inherent drawback of numerical solutions. This shows that both the solution algorithm and code are appropriately implemented in DFM.

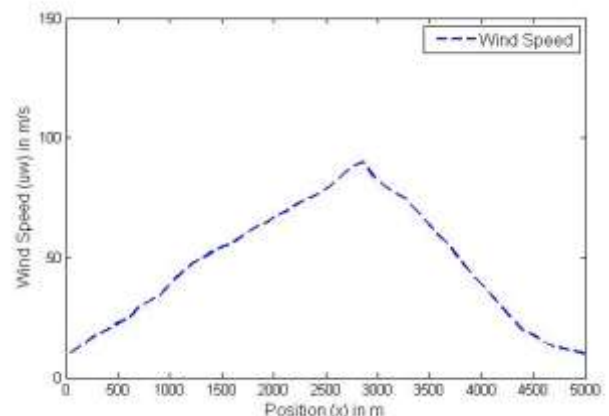


Fig. 6: Variable wind Speed  $u_w$ (m/s) in different positions  $x$ (m) along the channel for Case-3.

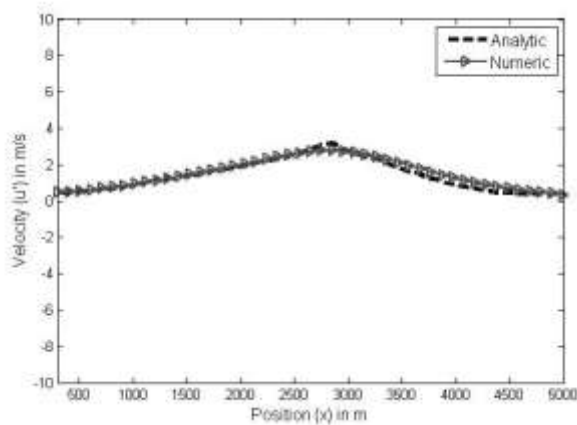


Fig. 7: Comparison of longitudinal velocity profile  $u$ (m/s) between the DFM and the numerical solution for Case-3.

#### 4. Model Calibration

By model calibration, we generally mean selecting the appropriate model parameters that represent experimental or field conditions [30]. DFM has two parameters that need to be calibrated. These are: wind drag coefficient  $C_w$  (see Equation 11) and Manning's  $n$  (see Equation 12). As mentioned before, the discretized Equations (34)-(37) are solved by coupling the DFM with Delft3D. The field application of DFM is made by coupling the field simulation result of Delft3D. To make DFM compatible with Delft3D, the same Manning's  $n$  is used both for DFM and Delft3D. As the solution algorithm between DFM and Delft3D is different, for wind drag coefficient  $C_w$ , an empirical equation is derived between  $C_w$  and wind velocity  $u_w$  which is used for different field applications of DFM. To derive this empirical equation, values of the wind drag coefficient used in a particular application of Delft3D (which is 0.002) and simulated water velocity from the same application of Delft3D is used. To make values of  $C_w$  used in Delft3D compatible with the DFM, following empirical equation is used:

$$C_w = 0.002 \times \left( \frac{u}{u_d} \right) \quad (38)$$

Where,  $C_w$  is a wind drag coefficient used as the calibration parameter of DFM,  $u$  is the simulated

water velocity for a particular application of Delft3D and  $u_d$  is the computed velocity for the same application of DFM. After a series of model runs with DFM, relation between wind drag coefficient  $C_w$  and wind velocity  $u_w$  is established and is shown in Fig. 8.

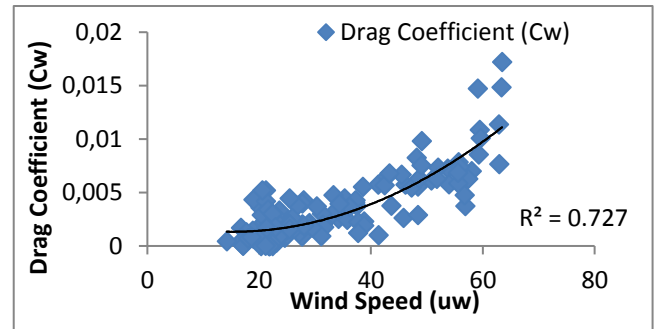


Fig. 8: Relation between wind drag coefficient  $C_w$  and wind velocity  $u_w$  computed by applying DFM

Using the relation in Fig. 8, following empirical equation between  $C_w$  and  $u_w$  is developed:

$$C_w = 0.000004u_w^2 + 0.002 \quad (39)$$

During subsequent model application by DFM, Equation (39) is used to compute the wind drag coefficient for specific cyclone wind speed represented by  $u_w$ .

The transfer of momentum from air to the ocean surface produces a wave field that imposes shear stress which ultimately causes the rise of water level [32]. The drag coefficient  $C_w$  controls the transfer of momentum from air to water surface in the governing momentum equation [33]. It mainly depends on wind speed. In modeling storm surge, this coefficient is a crucial parameter [34]. Past studies show that this coefficient either remains constant or increases with the increase of wind speed [35-40]. In the present study, it is found that the wind drag coefficient has a nonlinear relation with the wind speed (see Fig. 8 and Equation (50)).

#### 5. Model Validation

Model validation means the ability of the model to represent the real world for which the model is developed [30]. As real-world data of thrust force for any moving water mass is not available, validation of DFM is performed from two different perspectives. These are:

1. Validation of thrust force of DFM by comparing velocity-force curve generated for tsunami and cyclonic storm surge.
2. Validation of flow field of DFM with flow field simulation from calibrated and validated numerical model Delft 3D.

## 5.5 Validation with the tsunami force

Tsunami is a small amplitude wave created by lifting of water mass above the sea bottom due to rapture of the sea floor created mainly by earthquakes [41]. The potential energy of this displaced water mass converts into kinetic energy [41] and propagates with tremendous velocity (as high as 800 km/hr) in deep sea. This wave, when it reaches the coast, is slowed down but amplified due to shallow water effect and strikes the coastal structures with the same energy it had when it was created in the deep sea. On the other hand, cyclone generated storm surge is an elevated sea surface above the tide level due to lower atmospheric pressure and cyclonic wind. The storm surge acts simultaneously with tide and wind waves. The energy created due to storm surge is proportional to the tidal range of storm tide [42]. Similar to tsunamis, the storm surge is amplified near the coast due to the shallow water effect. The tsunami wave contains energy due to displacement of sea water mass above the sea-bed, whereas the storm surge contains energy created due to difference of sea surface elevation measured by tidal range of storm tide [41-42]. Energy of a tsunami wave is several times higher than a storm surge (water depth above sea-bed can be as high as 4000m, whereas, tidal range of a storm tide can vary between 6m to 7m depending on the tidal amplitude and strength of the cyclone). After reaching the coast, both the tsunami wave and storm surge strikes the coastal structure with a force which is directly proportional to the energy [43]. This means that after reaching the coast, the water mass created due to tsunami and moving with a certain velocity will exert more force on a coastal structure compared to a moving water mass moving with the same velocity but created due to cyclonic storm surge. The reason is – the moving water mass created by tsunami contains more energy compared to the moving water mass created by storm surge [41-42] and force is directly proportional to energy [43].

In the validation exercise of DFM force, we generate velocity-force curves for both tsunami and storm surge. For tsunamis, the velocity-force curve is generated by using the relation developed by Murata,

et al. (2011) [44] based on Japan tsunami study. They expressed the water velocity during tsunami wave propagation as  $u$  and the drag force of tsunami as  $F_d$  acting on coastal structures as:

$$u = 1.1\sqrt{gh} \quad (40)$$

$$F_d \cong 0.61\gamma_w C_d h^2 B \quad (41)$$

Where,  $\gamma_w$  is the specific weight of seawater,  $C_d$  is a drag coefficient,  $h$  is water depth and  $B$  is the breadth of a building in the flow direction. Velocity-force curve for tsunami wave is generated by calculating force with the following parameter values suggested by Murata, et al. (2011) [44]:

$$\gamma_w = 10.03 \text{ kN/m}^3$$

$$C_d = 2.2$$

$B = 1.0\text{m}$  to compute the force per unit length of the structure.

Values of  $h$  in Equation (41) is calculated from Equation (40) by assuming different ranges of velocity  $u$ .

For storm surge, the velocity-force curve is generated by applying DFM in the hypothetical channel which was used for model verification (Fig. 1). In this case, we used case-3 model setup (Fig. 6), but to get a reasonable range of force to generate velocity-force curve, we have used a higher range of wind speed compared to the wind speed range shown in Fig. 6. To generate velocity-force curves, different ranges of velocity are computed in different sections of the hypothetical channel by applying DFM. These velocities are used in Equation (29) to compute the force numerically. The numerical solution of Equation (29) is equivalent to the semi-analytical solution of Equation (32).

Comparison of velocity-force curve between tsunami and storm surge is shown in Fig. 9. The results show that for the same velocity, tsunami force is several times higher than storm surge force. With increasing velocity, this difference also increases. We have already discussed why tsunami force should be higher than storm surge force. The velocity-force curve in Fig. 9 shows that DFM realistically computes force due to cyclonic storm surge.

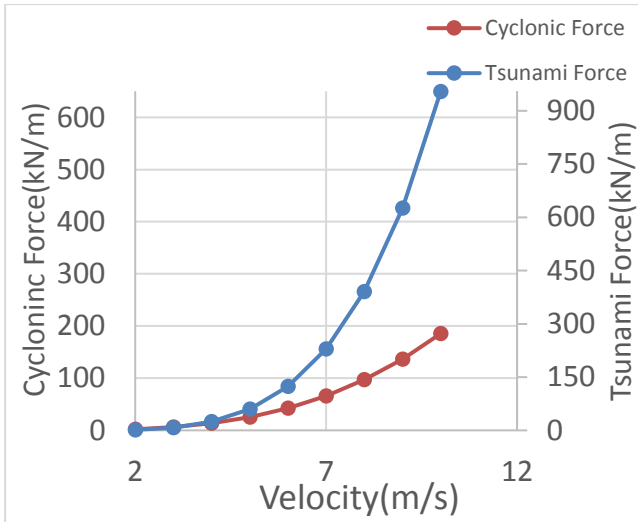


Fig. 9: Comparison of velocity-force curve between tsunami and storm surge.

### 5.6 Validation with Delft3D simulation

In this validation approach of DFM, the velocity field simulated by DFM is compared with the velocity field simulated by Delft 3D. The study area for this comparison is the coastal zone of Bangladesh (Fig. 10) for the tropical cyclone event SIDR that made landfall on the Bangladesh coast on November 15, 2007. Comparison of surge velocities between Delft 3D and DFM at the time of landfall is shown in Fig. 11.

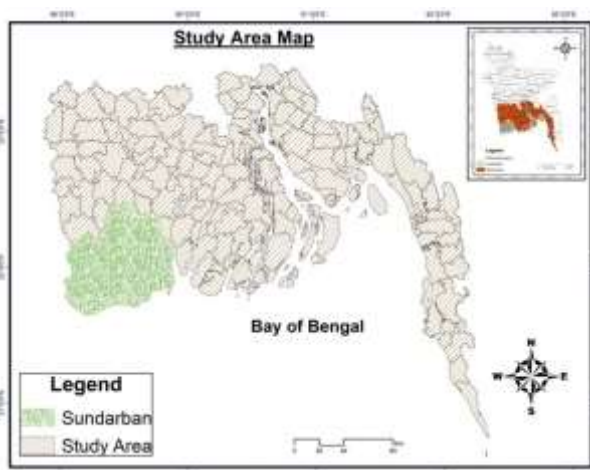


Fig. 10: Coastal zone of Bangladesh.

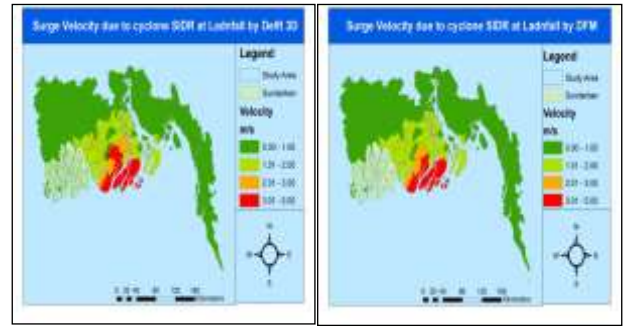


Fig. 11: Comparison of surge velocities between DFM and Delft 3D.

To quantify the visual qualitative color comparison, a one-to-one function is defined among the colors between the two maps. In this way, it is possible to quantify the overlapped color and deviated color between the two maps. The overlapped color shows the similarity, and the deviated color shows the dissimilarity between the maps. The comparison is shown in Table 1. The comparison shows that surge velocities computed by DFM is 97% similar to that computed by Delft3D. It is noted here that Delft3D applied in this study is a validated storm surge model in the coastal zone of Bangladesh [45]. From this perspective, this result shows the field validation of one important parameter of DFM.

Table 1: Map Comparison

Models	In Percentage (%)	
	Overlapped Colors	Deviated Colors
Delft3D – DFM	97%	3%

## 6. Model Application

The DFM model has numerous prospects in improving coastal resilience in particular and structural resilience in general. The model is not only able to compute dynamic thrust force due to cyclone generated storm surge, but also can compute the dynamic thrust force exerted by any moving water

mass on a structure in its flow path (for example due to tidal wave, wind wave, flows in ocean, estuaries and rivers, tsunami etc.). The output from the model can be used as one of the design criteria of infrastructures on which force is exerted by the moving water mass. As the DFM is capable of calculating spatial and temporal changes of thrust force, it can also be considered as one of the monitoring parameters of extreme climatic conditions related to moving water. As an illustration, the model is applied to compute dynamic thrust force due to tropical cyclone SIDR.

Tropical cyclone SIDR is considered as one of the devastating cyclones that made landfall on November 15, 2007 at the east of Sundarban in Bangladesh coast. During the time of landfall, the maximum wind speed of this cyclone was 215 km/hr [46]. This cyclone is believed to generate a maximum surge depth of 6m [47-48]. Simulated thrust force due to cyclone SIDR at the time of landfall is shown in Fig. 12. Table 2 shows the maximum thrust force at different coastal districts in Bangladesh (the district names are shown in Fig. 12) due to cyclone SIDR.

Table 2: Maximum thrust force at different coastal districts of Bangladesh due to cyclone SIDR.

District	Maximum thrust force (F) in kN/m
Patuakhali	110.5
Barguna	86.6
Bhola	54.1
Pirojpur	49.6
Jhalokati	44.5
Barisal	40.2

Bagerhat	33.2
Noakhali	17.9
Khulna	8.4
Chittagong	6.9
Lakshmipur	6.3
Cox's Bazar	4.8
Satkhira	4.3
Shariatpur	3.1
Narail	2.4
Gopalganj	2.2
Chandpur	2.1
Feni	1.9
Jessore	0.3

According to simulation results of DFM, the coastal districts of Patuakhali, Barguna, and Bhola (see Fig. 12) are impacted with a very high magnitude of thrust force (magnitude greater than 50 kN/m, see Table 2). In the post-disaster damage and loss assessment report, these districts are also identified as the worst affected coastal districts in terms of economic and infrastructure loss [47]. Due to anti-clockwise rotational impacts of cyclones in the northern hemisphere, locations on the right side of cyclone tracks are the most affected. According to DFM simulation, coastal districts of Patuakhali, Barguna and Bhola are the worst affected regions which are situated at the right side of the cyclone track and at

the same time close to the path of the cyclone track. On the other hand, although Pirojpur, Jhalokati and Bagerhat are situated close to the cyclone track (see Fig. 12), magnitude of thrust forces are relatively less in these districts (less than 50 kN/m) because these districts are located at the left side of the cyclone track. The red lines in Fig. 12 show the coastal embankments (locally known as polders) to protect the lands from surge waves. DFM simulated thrust force inside the protected land is only due to cyclone wind, not due to combined impact of cyclone wind and moving surge. But the thrust force in the unprotected land is due to combined impacts of moving surge and cyclone wind. Thrust force simulated by DFM can be applied to assess probability of failure of embankments during propagation of surge waves and possible damage of households both inside and outside the protected land. These data can also be used to further strengthen these structures or during construction of new structures in the coastal region.

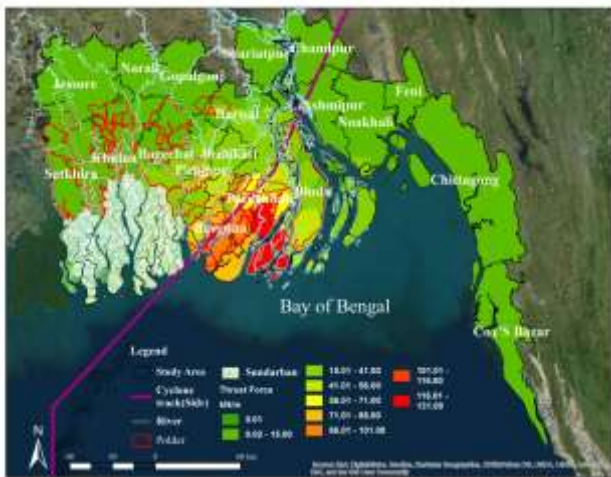


Fig. 12. Computed dynamic thrust force due to cyclone SIDR at the time of landfall in the coastal zone of Bangladesh.

## 7. Conclusion

A Dynamic Force Model (DFM) is developed by semi-analytically solving the Saint-Venant equations. The model can dynamically compute the thrust force due to any moving water mass including cyclone generated storm surge. As an analytical method, Variational Iteration Method (VIM) is used to solve the equations. During solution, steady and

uniform state of flow computed by Manning's equation is considered as an initial condition. Thrust force is computed from local and convective accelerations of moving water.

The model is verified (verification of solution algorithm and model code) by applying the model in a hypothetical channel on which wind is blowing. The computed water velocity by semi-analytical solution is compared with a finite difference solution. The verification results show systematic deviation of numerical solution from the analytical solution with increasing non-linearity in the system, which is an inherent drawback of numerical solutions. This shows the model algorithm and code are appropriately implemented. To apply the model in simulating dynamic thrust force due to cyclone generated storm surge, Manning's  $n$  and wind drag coefficients are used as the calibration parameters. For the DFM, an empirical equation is developed by relating wind drag coefficient with wind speed which can be used for any specific application (related to wind driven water flow) of the model. It is found that the wind drag coefficient increases non-linearly with the increase of wind speed. Thrust force computed by DFM is validated by comparing the model result with the tsunami data studied in Japan. On the other hand, surge velocity computed by DFM is validated by comparing the model result with the surge velocity computed by field validated numerical model Delft 3D. The verified, calibrated and validated DFM is applied to simulate dynamic thrust force in the Bangladesh zone due to tropical cyclone SIDR. This specific application shows the importance of thrust force as a parameter to assess performance of coastal infrastructure. DFM has the potential to be applied in engineering stability analysis of coastal infrastructures (for example embankments and building structures) to make these structures resilient against cyclone generated storm surge and tsunami. Next version of DFM will include the following:

1. DFM can be made independent by analytically solving the mass and momentum equations to compute the surge depth.
2. The zero-surge-depth problem needs to be solved mathematically.
3. DFM will be made a coupled module to the present version of Delft 3D. As Delft3D is open source, this coupling will make DFM to be used globally as part of Delft3D.

*Acknowledgement:*

*Collecting the bathymetry data for Delft3D model was supported by the 'ESPA Deltas (NE/J002755/1)' project funded by the ESPA programme, through Department for International Development (DFID), the Economic and Social Research Council (ESRC) and the Natural Environment Research Council (NERC), UK, and the National Water Resources Database hosted at Water Resources Planning Organization (WARPO), Ministry of Water Resources (MoWR), Government of the People's Republic of Bangladesh (GoB). The model development was supported by the DECCMA Project (Grant No. IDRC 107642), part of the Collaborative Adaptation Research Initiative in Africa and Asia (CARIAA), with financial support from the UK Government's DfID and the International Development Research Centre (IDRC), Canada, the WARPO Projects, 'Research on the Morphological processes under Climate Changes, Sea Level Rise and Anthropogenic Intervention in the coastal zone' and 'Research on Sediment Distribution and Management in South-West Region of Bangladesh' funded from MoWR, GoB and SATREPS (0510000000023) (funded by JST-JICA) through 'Research on Disaster Mitigation against Strom surges and floods in Bangladesh' are gratefully acknowledged.*

*This work is a part of author's Master's thesis, which is supported by DECCMA project which is further fine-tuned through different projects including the recent fellowship project in 2023 by Coalition for Disaster Resilient Infrastructures (CDRI). The views expressed in this work are those of the creators and do not necessarily represent those of DFID and IDRC, JICA, WARPO, CDRI or its Board of Governors*

*References:*

- [1] Solomon, Y. Modeling and simulation of tsunami and storm surge hydrodynamic loads on coastal bridge structures, 21st US-Japan Bridge Engineering Workshop, 2006.
- [2] Clark, R. R. Structural design aspects of a coastal building code. Coastal Engineering Proceedings, 1(18),1982.

[3] Pacheco, K.H. and Robertson, I.N., Evaluation of Tsunami Loads and other effect on Reinforced Concrete Buildings, <http://www.cee.hawaii.edu/wp-content/uploads/UHM-CEE-05-06.pdf>, 2005.

[4] Yeh, H., & Robertson, I. N. Development of design guideline for tsunami shelters. In Proc., First International Conference on Urban Disaster Reduction (1ICDR) (p. 2005)

[5] Palermo, D., Nistor, I., Nouri, Y., & Cornett, A. Tsunami loading of near-shoreline structures: a primer. Canadian Journal of Civil Engineering, 36(11), 1804-1815, 2009.

[6] Adomian, G., Stochastic System, New York : Academic Press, ©1983.

[7] Adomian, G., A Review of the Decomposition Method in Applied Mathematics. J. Math. Anal. Applic, 135:501-544, 1988.

[8] Liao, S., Homotopy analysis method: A new analytical technique for nonlinear problems” J. of Communications in Nonlinear Science and Numerical Simulation, [https://doi.org/10.1016/S1007-5704\(97\)90047-2](https://doi.org/10.1016/S1007-5704(97)90047-2), 1997.

[9] He, J.H. Variational iteration method for delay differential equations, Commun. Non-linear Sci. Numer. Simulation 2 (4) (1997) 235—236.

[10] He, J.H. Variational iteration approach to 2-spring system, Mech. Sci. Technol. 17(2) (1998) 221—223.

[11] He, J.H. Non-linear Oscillation with Fractional Derivative and its Approximation, Int. Conf. on Vibration Engineering 98, Dalian, China, 1988.J.-H. He / International Journal of Non-Linear Mechanics 34 (1999a) 699–708 707.

[12] He, J.H. Variational Iteration Method- a kind of non-linear analytical technique: some examples, International journal of non-linear Mechanics. Vol. 34, 1999b, pp.699-708

[13] Sinha, V. K., and Maroju, P.. New Development of Variational Iteration Method Using Quasilinearization Method for Solving Nonlinear Problems, Mathematics 11, no. 4: 935 (2023) <https://doi.org/10.3390/math11040935>

[14] Vidts, P.D. and White R.E. A Semi-Analytical Solution Method for Linear Partial Differential

Equations, Computer and Chemical Engineering, Vol. 16, No. IO/II, 1992, pp. 1007-1009.

[15] Mustapha, K.A., Furati, K.M., Knio, O.M. A Finite Difference Method for Space Fractional Differential Equations with Variable Diffusivity Coefficient. *Commun. Appl. Math. Comput.* 2, 671–688 (2020). <https://doi.org/10.1007/s42967-020-00066-6>

[16] Raisinghanian, M.D., Fluid Dynamics, chapter-12, p-928-930. India. 2003.

[17] Vreugdenhil, C.D. Numerical Method for Shallow water equations. Boston: kluwer Academic publishers, 1994.

[18] Kubatko, E., Development, Implementation and Verification of hp- Discontinuous Galerkin Models for shallow Water Hydrodynamics and Transport, PhD. Dissertation, 2005.

[19] Bessona, O., Kaneb, S. and Syc, M., On a 1D-Shallow Water Model: Existence of solution and numerical simulations, International Conference in Honor of Claude Lobry, 2007.

[20] Bulatov, O. V. Analytical and Numerical Riemann Solutions of the Saint Venant Equations for Forward and Backward Facing Step Flows, Computational Mathematics and Mathematical Physics, Faculty of Physics, Moscow State University, Moscow, 10.1134/S0965542514010047, 2013.

[21] Inokuti, M. General use of the Lagrange multiplier in non-linear mathematical physics, in: S. Nemat-Nasser (Ed.), Variational Method in the Mechanics of Solids, Pergamon Press, Oxford, 1978, pp. 156—162.

[22] Mungkasi, S., & Hari Wiryanto, L. Variational Iteration Solution to the Gravity Wave-Model Equations. *Journal of Physics: Conference Series*, 1007, 2018.

[23] Finlayson, B.A., The Method of Weighted Residuals and Variational Principles, Academic Press, New York, 1972.

[24] Nayfeh, A.H., Problems in Perturbation, Wiley, New York, 1985.

[25] Abdou, M.A. and Soliman, A.A. New Application of Variational Iteration Method, *Nonlinear Phenomena*, 211, 10.1016/j.physd.2005.08.002, 2005, pp.1-8.

[26] Hagedorn, P. Non-linear Oscillations (translated by Wolfram Stadler), Clarendon Press, Oxford, 1981.

[27] Holmes M.H. Perturbation Methods. In: Introduction to the Foundations of Applied Mathematics. Applied Mathematics, Springer, New York, NY, 2009.

[28] Chow, V. T. Open-channel hydraulics. McGraw-Hill Book Co., New York, N.Y., 1959.

[29] Deltares, Delft3D-Flow, Simulation of multi-dimensional hydrodynamic flows and transport phenomena, including sediments, User Manual, Version 3.15.34158, May 2014.

[30] Trucano, T.G., Swiler, L.P., Igusa, T., Oberkampf, W.L. and Pilch, M., Calibration, validation, and sensitivity analysis: What's what, *Reliability Engineering and System Safety*, 91 (2006) 1331–1357.

[31] Lundgren, L. and Mattsson, K. An efficient finite difference method for the shallow water equations. *Journal of Computational Physics*, 422(), 109784, doi:10.1016/j.jcp.2020.109784

[32] Powell, M.D., Vickery, P.J. and Reinhold, T.A., Reduced drag coefficient for high wind speeds in tropical cyclones, *Nature*, vol. 422, March 20. 2003, pp.279-283.

[33] Donelan, M.A., Drennan, W.M. and Katsaros, K.B. The Air–Sea Momentum Flux in Conditions of Wind Sea and Swell, *Journal of Physical Oceanography*, Vol(27), 1996, 10.1175/1520-0485(1997)027.

[34] Drews, C.W., Using wind set down and storm surge on Lake Fire to calibrate the air sea drag coefficient, *PLoS One*, 8, 101371/10.1371/journal.pone.0072510, 2013.

[35] Charnock, H., Wind stress on a Water Surface, *Quart. J. Roy. Meteorol. Soc.*, 81, 1955, 639-640.

[36] Large, W.G. and Pond, S., Open Ocean Momentum Flux Measurements in Moderate to Strong Winds, *J. Phys. Oceanogr.*, 11, 1981, pp.324-336.

[37] Smith, S.D. and Banke, E.G., Variation of the sea surface drag coefficient with wind speed. *Quart. J. Roy. Meteorol. Soc.*, 101, 1975, pp.665-673.

[38] Bender, M.A., Ginis, I., Tuleya, G.R., Thomas, B. and Marchok, T., The operational GFDL Coupled

Hurricane-Ocean Prediction System and a Summary of its performance, 3966, Mon. Wea. Rev., 135, 2007, 3965-3989.

[39] Kohno, M. and Higaki, M., The Development of a Storm Surge Model including the Effect of Wave set up for Operational Forecasting Meteorology and Geophysics. Papers in Meteorology and Geophysics, 57, 2006, 11-19, doi:10.2467/mripapers.57.11.

[40] Zhizhua, Z., Wang, Y., Yihong, D., Lianshou, C., Zhiqiu, G., On Sea Surface Roughness Parameterization and Its effect on tropical Cyclone Structure and Intensity. Advances in Atmospheric Sciences, vol. 27, no.1-4, 2010. pp.98-117.

[41] Dutykh Denys and Frederic Dias, Energy of tsunami waves generated by bottom motion, Proc. R. Soc. A (2009) 465, 725-744, doi:10.1098/rspa.2008.0332.

[42] Lewis, M.J. , Angeloudis, A., Robins, P.E. , Evans, P.S. and Neill, S.P. Influence of storm surge on tidal range energy, Energy, Volume 122, 2017, Pages 25-36, 2017, 0360-5442.

[43] Oetjen, J., Sundar, V., Venkatachalam, S. A comprehensive review on structural tsunami countermeasures. Nat Hazards 113, 2022, 1419-1449, <https://doi.org/10.1007/s11069-022-05367-y>

[44] Murata, S., Imamura, F., Katoh, K., Kawata, Y., Takahashi, S. and Takayama, T. TSUNAMI to survive from Tsunami, Advanced Series on Ocean Engineering, Vol (32), 2011.

[45] Haque, A., Kay, S. and Nichols, R.J. Present and future fluvial, tidal and storm surge flooding in coastal Bangladesh. Ecosystem Services for Well-Being in Deltas, Palgrave, 2018.

[46] Islam, A.K., Haque, M.S. and Bala, S.K. Hydrologic Characteristics of Floods in the Ganges-Brahmaputra-Meghna (GBM) delta, Natural Hazards, 54(3): 2010, 797-811. DOI: 10.1007/s11069-010-9504.

[47] GoB, Cyclone Sidr in Bangladesh: Damage, Loss and Needs Assessment for Disaster Recovery and Reconstruction. MoFDM, Dhaka, Bangladesh, 2008.

[48] Sakib, M., Nihal, F., Akter, R., Maruf, M., Akter, M., Haque, A., Rahman, M. —Afforestation as a Buffer against Storm Surge Flooding along the Bangladesh Coastal. 12th International Conference on Hydrosience & Engineering, 2016.

### **Contribution of Individual Authors to the Creation of a Scientific Article (Ghostwriting Policy)**

Marin Akter (Corresponding Author); She had major role to complete the task. Especially in Model development, validation, calibration and verification.

Mohammad Abdul Alim; He contributed on supervising.

Md. Manjurul Hossain; He contributed on programming on numerical code.

Kazi Samsunnahar Mita; she contribute on introduction writing.

Anisul Haque; he contributed on mathematical equations.

Munsur Rahman; He contributed on supervising.

Md. Rayhanur Rahman; He contributed on Introduction writing.

### **Sources of Funding for Research Presented in a Scientific Article or Scientific Article Itself**

Funding is not applicable

### **Conflict of Interest**

The authors have no conflicts of interest to declare that are relevant to the content of this article.

### **Creative Commons Attribution License 4.0 (Attribution 4.0 International, CC BY 4.0)**

This article is published under the terms of the Creative Commons Attribution License 4.0

[https://creativecommons.org/licenses/by/4.0/deed.en\\_US](https://creativecommons.org/licenses/by/4.0/deed.en_US)